# First-Principles Free-Energy Barriers for Photoelectrochemical Surface Reactions: Proton Abstraction at $TiO_2(110)$

Thomas Stecher,* Karsten Reuter, and Harald Oberhofer
*Chair for Theoretical Chemistry and Catalysis Research Center, Technische Universität München, Lichtenbergstr. 4, 85747 Garching, Germany*

(Received 12 September 2016; revised manuscript received 18 October 2016; published 29 December 2016)

We explicitly calculate the free-energy barrier for the initial proton abstraction in the water splitting reaction at rutile $TiO_2(110)$ through *ab initio* molecular dynamics. Combining solid-state embedding, an energy based reaction coordinate and state-of-the-art free-energy reconstruction techniques renders the calculation tractable at the hybrid density-functional theory level. The obtained free-energy barrier of approximately 0.2 eV, depending slightly on the orientation of the first acceptor water molecule, suggests a hindered reaction on the pristine rutile surface.

DOI: 10.1103/PhysRevLett.117.276001

In 1972 Fujishima and Honda first demonstrated the exceptional photocatalytic properties of titanium dioxide surfaces [1], creating hopes of an artificial form of photosynthesis, i.e., the direct use of solar energy to produce chemical fuels. While pure $TiO_2$ with its large band gap will not realistically be a suitable candidate material for this purpose, it remains an important prototype material. Understanding the Fujishima-Honda effect is seen as an important stepping stone on the way to more efficient catalyst materials. The main route in the computational study of this and related (photo-)electrochemical surface reactions has been to consider the thermodynamic stability of reaction intermediates, often within the framework of the computational hydrogen electrode (CHE) [2,3]. For the water splitting reaction, for instance, the following reaction steps are considered, with the asterisk denoting the catalytic surface: (In the case of anatase, somewhat modified mechanisms have recently been proposed [4,5]. In this Letter we choose to focus on rutile.)

$$H_2O + (*) \rightarrow HO^* + H^+(aq) + e^- \quad (1a)$$

$$HO^* \rightarrow O^* + H^+(aq) + e^- \quad (1b)$$

$$H_2O + O^* \rightarrow HOO^* + H^+(aq) + e^- \quad (1c)$$

$$HOO^* \rightarrow O_2 + (*) + H^+(aq) + e^-. \quad (1d)$$

The corresponding computation of minimum overpotentials, purely from the thermodynamics of the adsorbed reaction intermediates, has resulted in considerable insight regarding the energetic feasibility of potential catalyst materials [3,6].

Nevertheless, this type of CHE approach also has two important limitations: It is restricted to proton-coupled electron transfer (PCET) reaction mechanisms and it neglects any dynamical barriers, which may add to the purely thermodynamic overpotentials. Especially for photoelectrochemical reactions on semiconductors both of these assumptions have recently been called into question by new experimental [7–9] and theoretical results [10–13]. These point in particular to a much more substantial role of the reaction kinetics than previously considered. In this Letter we address this by establishing a general computational approach that allows us to explicitly calculate free-energy barriers through *ab initio* molecular dynamics simulations. This approach relies on a computationally efficient combination of methods enabling a full sampling of surface and solvent degrees of freedom along the reaction coordinate to yield a free energy profile in the presence of a reaction-driving electron hole. We thereby complement noteworthy earlier work in this direction. Li *et al.* [14] used the nudged elastic-band method to identify reaction mechanisms in related reactions. Selloni *et al.* [10] employed a mixture of dynamic and static sampling to determine the potential energy barrier of a proton transfer step in the water oxidation reaction. In an approach not unlike the one presented here, Schmickler and co-workers [15,16] determined free-energy surfaces of adsorption and electron transfer on metals from dynamical simulations based on a DFT parametrized Newns-Anderson model Hamiltonian. Finally, Chan and Nørskov [17] recently presented a constant-potential scheme for dynamical simulations of electrochemical interfaces on metals. This method is specifically designed to describe conditions at metal electrodes, and thus not easily adaptable to reaction conditions at semiconductor interfaces where trapped charge carriers drive the reaction [9].

We calculate the free-energy barrier for the proton transfer involved in the first step of the reaction scheme, Eq. (1), which is generally expected to be rate determining [3,6]. While this step is formally presented as a PCET reaction in the scheme, experiments indicate the electron transfer to be essentially barrierless [18]. We, therefore,

 

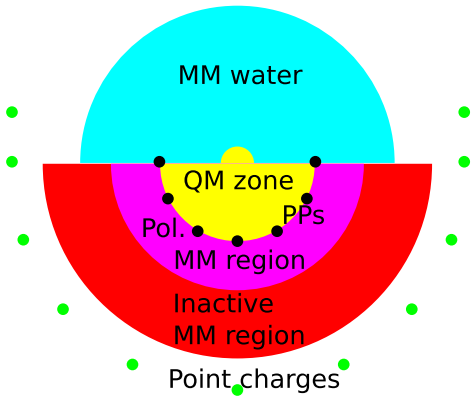


FIG. 1. Schematic illustration of the electrostatic QM/MM cluster embedding we use. The surface part of the QM zone (the embedded cluster) is surrounded by pseudopotentials (PPs), followed by a polarizable MM region and an inactive MM region. The embedding is capped off by a set of fitted point charges. On top of the surface are three QM water molecules followed by a hemisphere of 518 MM water molecules.

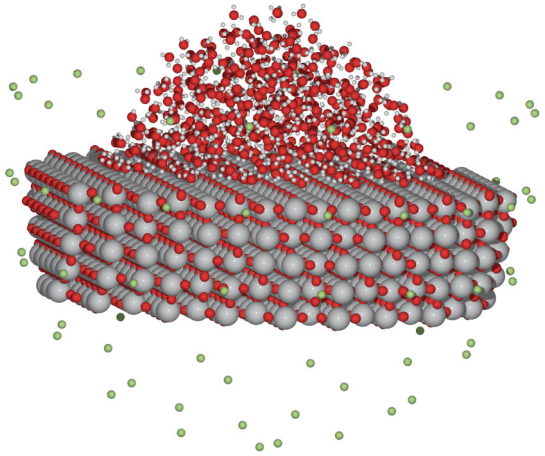

FIG. 2. Simulation snap shot of the full system (other than six point charges, which are placed further away).

focus on the proton transfer reaction on an already activated, i.e., positively charged, rutile $TiO_2(110)$ surface:

$$H_2O^{*+} \rightarrow HO^* + H^+(aq). \quad (2)$$

This reaction step was also investigated by Selloni and co-workers [10], albeit on an anatase rather than rutile surface, and with their work not going as far as calculating a free-energy profile. Attempting instead to explicitly calculate free-energy barriers for a system of this size and complexity requires one to find and take advantage of every possible efficiency available. In our approach, this starts with an electrostatic QM/MM cluster-embedding scheme for the surface model [19,20], schematically shown in Fig. 1. This depends critically on the presence of a large band gap, but in conjunction with a DFT-code built on an atom-centered basis set (FHI-aims [21,22]) enables efficient hybrid-level DFT calculations not achievable with standard periodic-boundary supercells. Incidentally, this also provides an alternative solution to the problem described (and solved) for metal electrodes by Chan and Nørskov [17], namely, barrier calculations at constant potential. Specifically, our calculations are based on a $Ti_{17}O_{34}$ cluster [23], surrounded by a layer of $Ti^{4+}$ pseudopotentials to prevent electronic spill-out effects. As shown in Fig. 1, this is followed by a polarizable MM region, in which the oxygen atoms are described by a core-shell model. This model is fitted to reproduce the high-frequency dielectric response of a periodic reference calculation, which ensures a proper description of the Fermi level. Closely following the recipe detailed in Ref. [24], embedding in an inactive outer region and capping with point charges finally recovers the correct Madelung potential of the periodic reference. On top of the surface we place a hemisphere of 521 water molecules, which we prevent from evaporating by a soft harmonic potential. Three reactive water molecules are included in the quantum region of the calculation. All others are described by the flexible SPC/Fw force field [25], which has been shown to reproduce the dielectric properties of water particularly well [26]. The interactions between the SPC water and the rutile surface rely on literature parameters [27]. Figure 2 shows a simulation snap shot of the full system, giving the reader an impression of the system set up. A limitation of the embedding scheme (at least for the present cluster size), is that the surface cannot be meaningfully relaxed and is kept frozen. This implies that we do not appropriately capture the static dielectric response of the solid.

As important as efficiency is for this calculation, it must not come at the expense of accuracy, in particular, with regard to the DFT functional. The literature is fairly clear that gradient-generalized approximations are inadequate both for the description of proton transfer reactions [28] (and indeed water [29]) as well as for the description of $TiO_2$ [30–32]. We, therefore, use the range-separated HSE06 functional [33,34] (with the standard screening parameter $\omega = 0.11$ bohr$^{-1}$), as other authors reporting results involving water on $TiO_2$ have done [30]. We use it in combination with the Tkatchenko-Scheffler correction [35] for dispersion interactions.

Perhaps most critical for an efficient calculation of the free-energy barrier is a judicious choice of the reaction coordinate. The positive charge transferred with the proton in our reaction induces a (slow) adaptation of the water structure surrounding it. If this is not reflected in the reaction coordinate (e.g., by using a simple geometric coordinate such as the difference between the lengths of the broken and newly formed bonds), very slow equilibration and convergence is observed. The recent work of Chen *et al.* [10] on a closely related system (anatase), for instance, can be interpreted as highlighting this

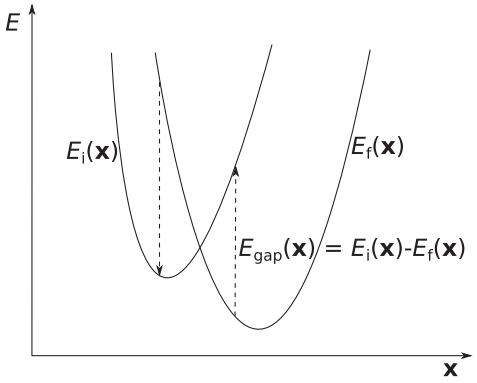


FIG. 3. Schematic explanation of the Energy Gap reaction coordinate involving the two diabatic potential energy surfaces $E_i(\mathbf{x})$ and $E_f(\mathbf{x})$, describing the initial and final state, respectively.

problem: because the surrounding water was not allowed to relax, the electron hole stayed permanently localized on the surface, even after dragging the proton all the way to the acceptor water molecule. In this Letter we, therefore, make use of the Energy Gap reaction coordinate [36,37]. It was originally proposed within the framework of empirical valence bond (EVB) theory [38], but is perhaps most intuitively understood as related to the reorganization energy of Marcus theory [39,40] (though the latter is of course a free energy). While it has found a number of applications within the EVB framework, particularly in the treatment of enzyme catalysis [41–43], to the best of our knowledge, the present work represents the first application of the Energy Gap reaction coordinate to an *ab initio* simulation beyond the semiempirical description of proton transfer in water [37]. The relatively straightforward idea is to use the energy difference between the diabatic initial and final states as the reaction coordinate, as this implicitly includes the solvent reorganization (Fig. 3). In practice, the diabats are approximated at the force-field level, the details of which we defer to the Supplemental Material [44]. It is worth pointing out that these force fields need not be particularly accurate: in Ref. [37] practically identical free-energy profiles were obtained over a wide range of Energy Gap parameters. An interesting puzzle was posed by the identity of the final state. As chemical intuition might suggest, we initially attempted to describe it as a hydronium ($H_3O^+$) ion in the first solvation shell of the *OH unit still attached to the surface; cf. Fig. 4(b). This does not, however, represent a metastable state and, as a result, an Energy Gap reaction coordinate based on it does not work. As illustrated in Fig. 4(c), we therefore describe the second diabatic state as a hydronium ion in the second solvation shell; i.e., the proton is abstracted and passed on (via the neighboring water) to a third water molecule. This is possibly also only an incomplete description of the final state. Yet, it is certainly sufficient to give a well-working reaction coordinate within the Energy Gap approach, covering both minima and the important free-energy barrier

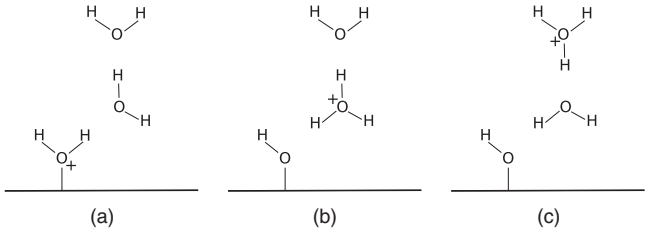


FIG. 4. Schematic illustration of the diabatic states employed for the Energy Gap reaction coordinate. (a) Initial state. (b) Unstable final state involving a hydronium ($H_3O^+$) ion in the first solvation shell. (c) Stable final state, used in the present calculations, with the $H_3O^+$ ion in the second solvation shell.

region. In a sense, this hypothetical state may be thought of as beyond the final state minimum. We will return to this mechanistic aspect below.

To avoid having to simulate the slow solvent rearrangement at the expensive QM/MM level, it is important to find a robust (pre-)equilibration strategy. The details of our protocol are once again deferred to the Supplemental Material [44], but the idea is to take advantage of the two force fields, developed for the reaction coordinate, to preequilibrate the bulk water. We use a simple linear mixture of the two force fields, running sequential equilibration trajectories, starting from a pure initial-state force field and arriving, in ten steps of 5 ps each, at the pure final-state force field. We can then perform QM/MM umbrella sampling [50] simulations from these starting geometries in parallel, each now only requiring another 250 fs of equilibration time. We employ harmonic umbrella potentials and use the sampled trajectories to derive one free-energy derivative [51] for each window. Finally, a free-energy profile is reconstructed using Gaussian process regression [52], a very efficient and principled approach, particularly suited to cases like ours, where the data (the sampled free-energy derivatives) are relatively noisy. We choose to focus most of our computing time (cf. the Supplemental Material [44] for details) on the first half of the free-energy profile to obtain the barrier height as accurately as possible. The remaining (downhill) part of the profile is also computed for completeness, but accepting larger statistical errors in this area.

In summary, our approach consists of the following steps. First, we set up a nonperiodic QM/MM model [24] of the $TiO_2$ surface and a large solvation hemisphere around the reaction center, describing the explicit MM water molecules with the flexible SPC/Fw force field [25] and interactions between the MM water and the rutile surface using literature parameters [27]. Then, using harmonic umbrella potentials, we stratify the free-energy profile into 13 windows along a Marcus-theory inspired Energy Gap reaction coordinate, which is obtained from two specifically fitted force fields. Each window is preequilibrated at the MM level, with force field parameters linearly interpolated between initial and final configurations. Then, 1–1.5 ps-long QM/MM trajectories are run in each window to sample each portion of the

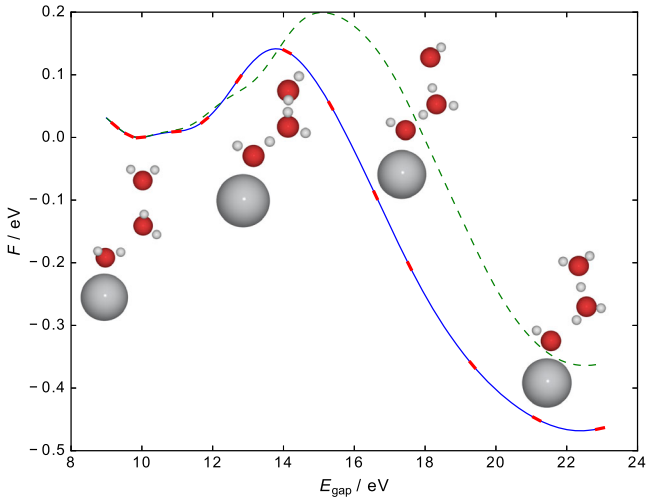


FIG. 5. Reconstructed free-energy profiles for the proton transfer reaction. The profile depends slightly on the orientation of the middle (first acceptor) water molecule: one of its hydrogen atoms pointing towards the surface (case 1, solid line) or not (case 2, dashed line). The red dashes show the free-energy derivatives obtained in the umbrella-sampling calculations. The insets show representative geometries along the reaction coordinate for case 1, which provides a lower estimate of the free-energy barrier.

reaction coordinate. Information from all windows is finally integrated into a full free-energy profile using Gaussian process regression.

As shown in Fig. 5 the resulting free-energy profile is found to depend somewhat on the orientation of the middle (first acceptor) water molecule, in particular, on whether one of its hydrogen atoms points towards the surface (case 1) or not (case 2). If the water molecule does interact with the surface, the barrier appears slightly earlier and seems to be a little bit lower on the order of a few tens of meV. In an infinitely long calculation, both states would be sampled extensively and one properly weighted profile obtained. In the following, we concentrate on the free-energy profile obtained for case 1, which provides a lower estimate for the barrier of such a properly weighted profile. This estimate amounts to $0.14 \pm 0.03$ eV, which, together with a basis set correction of $0.06 \pm 0.02$ eV (cf. the Supplemental Material [44]) gives the approximately 0.2 eV quoted above. While 200 meV may not sound large (and the inclusion of nuclear quantum effects would conceivably lead to a marginally lower value), it is important to recall that the calculated kinetic barrier adds to the thermodynamic barrier previously determined for this rate-limiting reaction step [6]. The thermodynamic barrier was already marginally larger than the rutile band gap, which suggests photogenerated electron holes to be energetically insufficient to drive the reaction. While previously one may have argued that this result was still within the uncertainty of the DFT functional, the present additional kinetic barrier further strengthens it. Mechanistically, we therefore conclude that a perfectly pristine rutile $TiO_2(110)$ surface is not able to photoelectrically split water. The Fujishima-Honda effect will therefore have to be explained otherwise, for instance, in terms of more reactive surface defects [53].

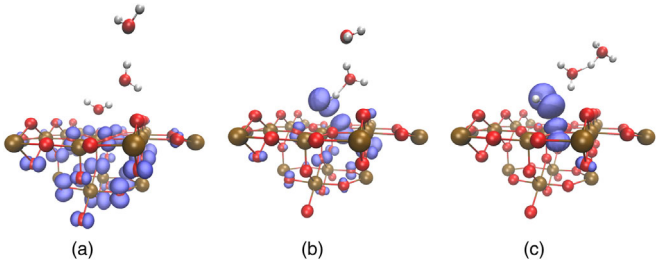


FIG. 6. Spin densities (0.01 a.u. contours) for representative structures of the initial state (a), the barrier (b), and the final state (c) along the proton abstraction profile.

For example, it has been shown that surface oxygen vacancies, which are highly abundant under most conditions, aid in the localization of electron holes [24]. Changes in the hole level can then directly translate into changes of reaction free energies [3]. Thus, while the influence of such vacancies on kinetic barriers is still completely unknown, a more downhill step in terms of free energy differences between initial and final state can be expected to directly improve the reactivity of the surface. Future exploration of kinetic barriers on defected surfaces is therefore highly desirable.

Methodologically, we note that our estimated free-energy barrier is right at the bottom of the range estimated by Selloni and co-workers [10], even though their estimate is for the more reactive anatase phase of $TiO_2$. In our view, our lower barrier value is a direct consequence of appropriately considering the solvent degrees of freedom very much as part of the reaction coordinate. We note further that the Energy Gap reaction coordinate is defined entirely in terms of the nuclear degrees of freedom; i.e., we put no restrictions on the electronic degrees of freedom. Nonetheless, it is interesting to analyze the behavior of the electron-hole along the reaction. To this end we calculate the spin densities for three representative snapshots along the sampled trajectories at the initial state, the barrier, and the final state. The results are shown in Fig. 6. Initially, the hole is clearly confined to the surface, before it gradually moves to the adsorbate where it eventually localizes.

The free energy profile also exhibits some interesting features beyond the barrier. It can be clearly seen that, as anticipated above, a hydronium ion in the first solvation shell does not correspond to a metastable state, but is very much part of the barrier region. It can also be observed, however, that a hydronium ion in the second solvation shell, though perfectly adequate for use in the Energy Gap reaction coordinate, is not an accurate description of the second minimum, either. Rather, this looks much more like a Zundel ion; i.e., the excess proton is shared between two water molecules. This is in agreement with the more recent literature on the topic [54,55].

Of course, the merit of the calculation presented in this Letter is as much about demonstrating a path to obtaining free-energy barriers in these challenging systems, as it is about the numbers themselves. While improvements can undoubtedly still be made—a larger quantum zone would be desirable (cf. also the Supplemental Material [44]), possibly chosen in an adaptive framework [56], nuclear quantum effects might be considered, etc.—the present framework nevertheless represents a reliable, transferable and, given the task, affordable framework for further efforts. Not least will it be useful as an accurate benchmark for more approximate schemes to be tested against.

We thank Matthias Kick and Daniel Berger for help with the embedded cluster calculations and Letif Mones for helpful discussions about the Energy Gap reaction coordinate. T. S. is supported by the Deutsche Forschungsgemeinschaft (STE 2438/1-1). K. R. and H. O. gratefully acknowledge support from the state of Bavaria via the "Solar technologies go hybrid" initiative.

*thomas.stecher@tum.de

[1] A. Fujishima and K. Honda, Nature (London) **238**, 37 (1972).
[2] J. K. Nørskov, J. Rossmeisl, A. Logadottir, L. Lindqvist, J. R. Kitchin, T. Bligaard, and H. Jónsson, J. Phys. Chem. B **108**, 17886 (2004).
[3] Á. Valdés, Z. W. Qu, G. J. Kroes, J. Rossmeisl, and J. K. Nørskov, J. Phys. Chem. C **112**, 9872 (2008).
[4] C. Di Valentin, J. Phys. Condens. Matter **28**, 074002 (2016).
[5] Y.-F. Li and A. Selloni, ACS Catal. **6**, 4769 (2016).
[6] H. Oberhofer and K. Reuter, J. Chem. Phys. **139**, 044710 (2013).
[7] J. Tang, J. R. Durrant, and D. R. Klug, J. Am. Chem. Soc. **130**, 13885 (2008).
[8] A. J. Cowan, J. Tang, W. Leng, J. R. Durrant, and D. R. Klug, J. Phys. Chem. C **114**, 4208 (2010).
[9] A. J. Cowan and J. R. Durrant, Chem. Soc. Rev. **42**, 2281 (2013).
[10] J. Chen, Y.-F. Li, P. Sit, and A. Selloni, J. Am. Chem. Soc. **135**, 18774 (2013).
[11] M. T. M. Koper, Chem. Sci. **4**, 2710 (2013).
[12] A. V. Akimov, A. J. Neukirch, and O. V. Prezhdo, Chem. Rev. **113**, 4496 (2013).
[13] A. J. Göttle and M. T. M. Koper, Chem. Sci., doi:10.1039/C6SC02984A (2017).
[14] P. Li, G. Henkelman, J. A. Keith, and J. K. Johnson, J. Phys. Chem. C **118**, 21385 (2014).
[15] E. Santos, A. Lundin, K. Pötting, P. Quaino, and W. Schmickler, Phys. Rev. B **79**, 235436 (2009).
[16] L. M. C. Pinto, P. Quaino, M. D. Arce, E. Santos, and W. Schmickler, Chem. Phys. Chem. **15**, 2003 (2014).
[17] K. Chan and J. K. Nørskov, J. Phys. Chem. Lett. **6**, 2663 (2015).
[18] A. J. Cowan, C. J. Barnett, S. R. Pendlebury, M. Barroso, K. Sivula, M. Grätzel, J. R. Durrant, and D. R. Klug, J. Am. Chem. Soc. **133**, 10134 (2011).
[19] D. Berger, A. J. Logsdail, H. Oberhofer, M. R. Farrow, C. R. A. Catlow, P. Sherwood, A. A. Sokol, V. Blum, and K. Reuter, J. Chem. Phys. **141**, 024105 (2014).
[20] A. A. Sokol, S. T. Bromley, S. A. French, C. R. A. Catlow, and P. Sherwood, Int. J. Quantum Chem. **99**, 695 (2004).
[21] V. Blum, R. Gehrke, F. Hanke, P. Havu, V. Havu, X. Ren, K. Reuter, and M. Scheffler, Comput. Phys. Commun. **180**, 2175 (2009).
[22] X. Ren, P. Rinke, V. Blum, J. Wieferink, A. Tkatchenko, A. Sanfilippo, K. Reuter, and M. Scheffler, New J. Phys. **14**, 053020 (2012).
[23] S. C. Ammal and A. Heyden, J. Chem. Phys. **133**, 164703 (2010).
[24] D. Berger, H. Oberhofer, and K. Reuter, Phys. Rev. B **92**, 075308 (2015).
[25] Y. Wu, H. L. Tepper, and G. A. Voth, J. Chem. Phys. **124**, 024503 (2006).
[26] G. Raabe and R. J. Sadus, J. Chem. Phys. **134**, 234501 (2011).
[27] M. Předota, A. V. Bandura, P. T. Cummings, J. D. Kubicki, D. J. Wesolowski, A. A. Chialvo, and M. L. Machesky, J. Phys. Chem. B **108**, 12049 (2004).
[28] G. F. Mangiatordi, E. Brémond, and C. Adamo, J. Chem. Theory Comput. **8**, 3082 (2012).
[29] M. J. Gillan, D. Alfè, and A. Michaelides, J. Chem. Phys. **144**, 130901 (2016).
[30] R. V. Mom, J. Cheng, M. T. M. Koper, and M. Sprik, J. Phys. Chem. C **118**, 4095 (2014).
[31] J. Cheng, X. Liu, J. A. Kattirtzi, J. VandeVondele, and M. Sprik, Angew. Chem., Int. Ed. Engl. **53**, 12046 (2014).
[32] H. Sun, D. J. Mowbray, A. Migani, J. Zhao, H. Petek, and A. Rubio, ACS Catal. **5**, 4242 (2015).
[33] J. Heyd, G. E. Scuseria, and M. Ernzerhof, J. Chem. Phys. **124**, 219906 (2006).
[34] A. V. Krukau, O. A. Vydrov, A. F. Izmaylov, and G. E. Scuseria, J. Chem. Phys. **125**, 224106 (2006).
[35] A. Tkatchenko and M. Scheffler, Phys. Rev. Lett. **102**, 073005 (2009).
[36] L. Mones, P. Kulhánek, I. Simon, A. Laio, and M. Fuxreiter, J. Phys. Chem. B **113**, 7867 (2009).
[37] L. Mones and G. Csányi, J. Phys. Chem. B **116**, 14876 (2012).
[38] A. Warshel and R. M. Weiss, J. Am. Chem. Soc. **102**, 6218 (1980).
[39] R. A. Marcus, Annu. Rev. Phys. Chem. **15**, 155 (1964).
[40] R. A. Marcus, J. Chem. Phys. **24**, 966 (1956).
[41] A. Warshel, P. K. Sharma, M. Kato, Y. Xiang, H. Liu, and M. H. M. Olsson, Chem. Rev. **106**, 3210 (2006).
[42] L. Mones, W.-J. Tang, and J. Florián, Biochemistry **52**, 2672 (2013).
[43] A. Labas, E. Szabo, L. Mones, and M. Fuxreiter, Biochimica et Biophysica Acta (BBA)—Proteins and Proteomics **1834**, 908 (2013).
[44] See Supplemental Material at http://link.aps.org/supplemental/10.1103/PhysRevLett.117.276001 for computational details, which includes Refs. [45–49].
[45] M. Sprik, J. Phys. Chem. **95**, 2283 (1991).
[46] A. Jones and B. Leimkuhler, J. Chem. Phys. **135**, 084125 (2011).

[47] B. Leimkuhler, E. Noorizadeh, and F. Theil, J. Stat. Phys. **135**, 261 (2009).
[48] R. W. Zwanzig, J. Chem. Phys. **22**, 1420 (1954).
[49] C. E. Rasmussen and C. K. I. Williams, *Gaussian Processes for Machine Learning*, Adaptive Computation and Machine Learning Series (MIT Press, Cambridge, 2006).
[50] G. M. Torrie and J. P. Valleau, Chem. Phys. Lett. **28**, 578 (1974).
[51] J. Kästner and W. Thiel, J. Chem. Phys. **123**, 144104 (2005).
[52] T. Stecher, N. Bernstein, and G. Csányi, J. Chem. Theory Comput. **10**, 4079 (2014).
[53] C. L. Pang and G. Thornton, *Defects at Oxide Surfaces* (Springer, New York, 2015), p. 429.
[54] E. S. Stoyanov, I. V. Stoyanova, and C. A. Reed, Chem. Sci. **2**, 462 (2011).
[55] C. A. Reed, Acc. Chem. Res. **46**, 2567 (2013).
[56] N. Bernstein, C. Várnai, I. Solt, S. A. Winfield, M. C. Payne, I. Simon, M. Fuxreiter, and G. Csányi, Phys. Chem. Chem. Phys. **14**, 646 (2012).